CMS Physics Analysis Summary

Contact: cms-pag-conveners-susy@cern.ch 2014/02/18

Search for electroweak production of higgsinos in channels with two Higgs bosons decaying to b quarks in pp collisions at 8 TeV

The CMS Collaboration

Abstract

A search is presented for the electroweak pair production of higgsinos, both of which decay to a Higgs boson and an almost massless, lightest supersymmetric particle (LSP). Each Higgs boson is reconstructed in its decay to a bottom quark-antiquark pair. The LSPs are presumed to be undetected, leading to missing transverse energy. The data sample corresponds to an integrated luminosity of 19.3 fb^{-1} of proton-proton collisions collected in 2012 by the CMS experiment at the LHC at a center-of-mass energy of 8 TeV. For higgsino masses between about 270 and 350 GeV, the expected 95% confidence-level upper limits on the cross section reach the level of the predicted production cross section. Because of a slight excess in the observed number of events compared to the estimated background, no exclusion is obtained for any higgsino mass value.

1 Introduction

Supersymmetry (SUSY) [1–8], one of the most widely considered extensions of the standard model (SM) of particle physics, predicts unification of the strong, weak, and electromagnetic forces, stabilizes the Higgs boson mass at the electroweak energy scale, and may provide a dark matter candidate. SUSY postulates that each SM particle is paired with a SUSY partner from which it differs in spin by one-half unit, with otherwise identical quantum numbers. For example, squarks, gluinos, and higgsinos are the SUSY partners of quarks, gluons, and Higgs bosons, respectively. In SUSY, neutral higgsinos mix with the SUSY partners of the photon and Z boson to form neutralinos $\widetilde{\chi}^0$, while charged higgsinos mix with the SUSY partners of the W boson to form charginos $\widetilde{\chi}^{\pm}$. In so-called natural scenarios of SUSY [9–11], top squarks, bottom squarks, gluinos, and higgsino-enriched neutralinos and charginos are expected to be relatively light, enhancing their production cross sections.

Extensive searches for gluinos, squarks, neutralinos, and charginos have been performed at the Large Hadron Collider (LHC) at CERN, but without uncovering evidence for their production. The recent discovery [12–14] of a Higgs boson with a mass around 126 GeV opens the possibility for a new type of search [15–17] based on the requirement of one or more Higgs bosons in the final state. A well-motivated possibility [18], arising in gauge-mediated-SUSY-breaking scenarios [18, 19], concerns the electroweak pair production of the $\widetilde{\chi}^0_1$, $\widetilde{\chi}^0_2$ or $\widetilde{\chi}^{\pm}_1$ particles, where $\widetilde{\chi}^0_1$ and $\widetilde{\chi}^0_2$ are the two lightest neutralinos and $\widetilde{\chi}^{\pm}_1$ is the lightest chargino. In this scenario, all three of these particles are higgsino-enriched and are approximately mass-degenerate. We therefore refer to the $\widetilde{\chi}^0_1$, $\widetilde{\chi}^0_2$, and $\widetilde{\chi}^{\pm}_1$ as higgsinos, with $\widetilde{\chi}^0_1$ the lightest higgsino. Any combination of two of these three particles can be pair-produced, except that $\widetilde{\chi}^0_1\widetilde{\chi}^0_1$ ($\widetilde{\chi}^0_2\,\widetilde{\chi}^0_2$) production is not allowed if the $\widetilde{\chi}^0_1$ ($\widetilde{\chi}^0_2$) is a pure higgsino. The $\widetilde{\chi}^0_2$ and $\widetilde{\chi}^{\pm}_1$ higgsinos decay to the $\widetilde{\chi}^0_1$ higgsino plus low transverse-momentum (p_{T}) SM particles. The $\widetilde{\chi}^0_1$ higgsino decays according to $\widetilde{\chi}^0_1 \to \mathrm{H}\widetilde{\mathrm{G}}$, with H a Higgs boson and $\widetilde{\mathrm{G}}$ a gravitino. The gravitino, which is nearly massless, is the lightest SUSY particle (LSP).

In this note, we present a search for the electroweak pair production of $\widetilde{\chi}^0_1$ higgsinos through the above scenario. Each $\widetilde{\chi}^0_1$ particle is produced either directly or through the decay of a $\widetilde{\chi}^0_2$ or $\widetilde{\chi}^{\pm}_1$ higgsino. An event diagram is shown in Fig. 1. We search in the channel in which both Higgs bosons decay to a bottom quark-antiquark ($\mathrm{b\bar{b}}$) pair, representing the most probable Higgs boson decay mode [20]. (We assume the Higgs bosons to have SM properties.) The two LSPs in an event are presumed to be weakly interacting and to escape without detection, leading to potentially large values of missing transverse energy $E_{\mathrm{T}}^{\mathrm{miss}}$.

The data, corresponding to an integrated luminosity of 19.3 fb^{-1} of proton-proton (pp) collisions collected at $\sqrt{s} = 8$ TeV, were recorded with the Compact Muon Solenoid (CMS) detector at the LHC in 2012. The signal consists of a final state with either exactly four or exactly five jets, no identified τ lepton, no identified isolated electron, muon, or charged track, and large values of the $E_{\mathrm{T}}^{\mathrm{miss}}$-significance variable $\mathcal{S}_{\mathrm{MET}}$ [21], where $\mathcal{S}_{\mathrm{MET}}$ represents a χ^2 difference between the observed result for $E_{\mathrm{T}}^{\mathrm{miss}}$ and the $E_{\mathrm{T}}^{\mathrm{miss}} = 0$ hypothesis. Because it accounts for finite jet resolution on an event-by-event basis, $\mathcal{S}_{\mathrm{MET}}$ provides better discrimination between signal and background events than does $E_{\mathrm{T}}^{\mathrm{miss}}$ itself, especially for background events that contain large values of $E_{\mathrm{T}}^{\mathrm{miss}}$ as a consequence of detector mismeasurements. We attempt to reconstruct the two $\mathrm{H} \to \mathrm{b\bar{b}}$ candidate decays using the four jets most consistent with the bottom-quark jet (b jet) hypothesis.

The background from SM processes is estimated using data control samples. The dominant background arises from top-quark-antiquark-pair ($\mathrm{t\bar{t}}$) events, especially $\mathrm{t\bar{t}}$ events in which one

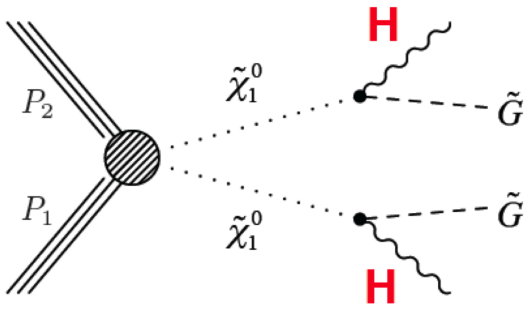

Figure 1: Event diagram for the SUSY scenario considered in this analysis, with $\tilde{\chi}_1^0$ the lightest higgsino and $\widetilde{G}$ a gravitino. Each Higgs boson H decays to a $b\bar{b}$ pair.

top quark decays hadronically while the other decays semileptonically, where the lepton is not identified and the neutrino is a source of genuine E_T^{miss}. Other backgrounds arise from the production of events with a single-top quark, a W boson in association with jets (W+jets), a Z boson in association with jets (Z +jets), multiple jets produced through the strong interaction (QCD multijet), and rare processes such as $t\bar{t}V$, VV, WH, ZH, and $t\bar{t}H$ combinations, with V a W or Z boson. The QCD multijet category excludes events in the other categories. For events with a top quark or W boson, significant E_T^{miss} can arise if a W boson decays into a neutrino and an unidentified charged lepton. For events with a Z boson, significant E_T^{miss} can arise if the Z boson decays to two neutrinos. For QCD multijet and all-hadronic $t\bar{t}$ events, significant E_T^{miss} can arise if a charm or bottom quark undergoes semileptonic decay, but the principal source of E_T^{miss} is the mismeasurement of jet transverse momentum.

2 Detector and trigger

A detailed description of the CMS detector is given elsewhere [22]. The CMS coordinate system is defined with the origin at the center of the detector and the z axis along the direction of the counterclockwise beam. The transverse plane is perpendicular to the beam axis, with ϕ the azimuthal angle (measured in radians), θ the polar angle, and $\eta = -\ln[\tan(\theta/2)]$ the pseudorapidity. A superconducting solenoid provides an axial magnetic field of 3.8 T. Within the field volume are a silicon pixel and strip tracker, a crystal electromagnetic calorimeter, and a brass-scintillator hadron calorimeter. The tracking system is completed with muon detectors based on gas-ionization chambers embedded in the steel flux-return yoke outside the solenoid. The tracking system extends to $|\eta| < 2.5$ and the calorimeters to $|\eta| < 3.0$. Steel-and-quartz-fiber forward calorimeters cover $3 < |\eta| < 5$. The near-hermeticity of the detector permits accurate measurements of energy balance in the transverse plane.

Events are selected using the logical "OR" of several trigger conditions. One trigger requires the presence of at least two jets and at least one tagged b jet, with a minimum threshold for E_T^{miss}. Another trigger is based on E_T^{miss} only, but with a higher threshold. The trigger efficiency, determined from data, is the probability for a signal event to satisfy the trigger conditions. In our analysis, the data are examined in exclusive intervals of the $\mathcal{S}_{MET}$ variable. We find that the trigger efficiency rises from around 55% for $\mathcal{S}_{MET} \approx 30$, which is the lowest $\mathcal{S}_{MET}$ value considered in the analysis, to a plateau of around 95% for $\mathcal{S}_{MET} \gtrsim 100$. The trigger is fully efficient with respect to the jet-p_T and b-jet-tagging requirements of the analysis. Corrections are applied to account for the trigger efficiencies and their corresponding uncertainties.

3 Baseline event selection

Physics objects are defined with the particle flow (PF) method [23], which is used to reconstruct and identify charged and neutral hadrons, electrons (with associated bremsstrahlung photons), muons, and photons, using an optimized combination of information from CMS subdetectors. Hadronically decaying τ leptons are reconstructed using PF objects (we use the HPS τ-lepton reconstruction algorithm [24] with "loose" identification requirements). The event primary vertex is taken to be the reconstructed vertex with the largest sum of charged-track p_{T}^2 values. The primary vertex is required to contain at least four charged tracks and to lie within 24 cm of the origin in the direction along the beam axis and 2 cm in the perpendicular direction. Charged particles emanating from a vertex other than the primary vertex are not considered. In this way, charged particles associated with extraneous pp interactions within the same or a nearby bunch crossing ("pileup") are disregarded. The PF objects serve as input for jet reconstruction, based on the anti-k_{T} algorithm [25] with a distance parameter of 0.5. Jet corrections are applied as a function of p_{T} and η to account for residual effects of non-uniform detector response. Contributions to an individual jet's p_{T} from pileup, due, e.g., to neutral particles, are subtracted using the jet area method described in Ref. [26]. Jets from pileup interactions are suppressed through requirements on the compatibility of the jet's charged particle constituents with the primary vertex. Jets are required to satisfy basic quality criteria (jet ID) and to lie within the fiducial region defined by $p_{\mathrm{T}} > 20\,\mathrm{GeV}$ and $|\eta| < 2.4$.

The missing transverse energy $E_{\mathrm{T}}^{\mathrm{miss}}$ is defined as the modulus of the vector sum of the transverse momenta of all PF objects. The $E_{\mathrm{T}}^{\mathrm{miss}}$ vector is the negative of that same vector sum.

The principal visible objects in signal events are the four b jets from the decay of the two Higgs bosons (Fig. 1). Additional jets may arise from initial-state radiation, final-state radiation, or pileup interactions. To select events, we require:

- exactly four or exactly five jets, where the two highest p_{T} jets satisfy $p_{\mathrm{T}} > 50\,\mathrm{GeV}$;
- $E_{\mathrm{T}}^{\mathrm{miss}}$ significance [21] $\mathcal{S}_{\mathrm{MET}} > 30$;
- no identified, isolated electron or muon candidate with $p_{\mathrm{T}} > 10\,\mathrm{GeV}$; electron candidates are restricted to $|\eta| < 2.5$ and muon candidates to $|\eta| < 2.4$;
- no hadronically decaying τ lepton candidate with $p_{\mathrm{T}} > 20\,\mathrm{GeV}$ and $|\eta| < 2.4$;
- no isolated charged-particle track with $p_{\mathrm{T}} > 10\,\mathrm{GeV}$ and $|\eta| < 2.4$;
- $\Delta\phi_{\mathrm{min}} > 0.5$ for events with $30 < \mathcal{S}_{\mathrm{MET}} < 50$ and $\Delta\phi_{\mathrm{min}} > 0.3$ for $\mathcal{S}_{\mathrm{MET}} > 50$, where $\Delta\phi_{\mathrm{min}}$ is the smallest difference in ϕ between the $E_{\mathrm{T}}^{\mathrm{miss}}$ vector and any jet in the event; for the $\Delta\phi_{\mathrm{min}}$ calculation we use less restrictive criteria for jets compared with the standard criteria: $|\eta| < 5.0$, no rejection of jets from pileup interactions, and no jet ID requirements, with all other conditions unchanged.

The isolated-track requirement eliminates events with a single-prong τ lepton or an isolated electron or muon in cases where the lepton is not identified. Electrons, muons, and tracks are considered isolated if the scalar sum of the p_{T} values of charged hadrons (for electrons and muons, also photons and neutral hadrons) surrounding the lepton or track within a cone of radius $\sqrt{(\Delta\eta)^2 + (\Delta\phi)^2} = 0.3$ (0.4 for muons), divided by the lepton or track p_{T} value itself, is less than 0.15, 0.20, and 0.10, respectively. The $\Delta\phi_{\mathrm{min}}$ restriction eliminates QCD multijet and all-hadronic $\mathrm{t\bar{t}}$ events, whose contribution is expected to be large at small values of $\mathcal{S}_{\mathrm{MET}}$. The use of less restrictive jet requirements for the $\Delta\phi_{\mathrm{min}}$ calculation yields more efficient rejection of these backgrounds.

4 Tagging of b jets and b-jet samples

The identification of b jets is performed using the combined secondary vertex (CSV) algorithm [27, 28], which computes a discriminating variable for each jet based on quantities that are sensitive to b-jet production such as displaced secondary vertices, tracks with large impact parameters, and kinematical variables like jet mass. We make use of three operating points for the algorithm, denoted loose, medium, and tight. These three working points yield misidentification probabilities for light-parton jets of approximately 10%, 1%, and 0.1%, respectively, for jet p_T values around 80 GeV, as determined from samples of multijet and $\mathrm{t\bar{t}}$ events [28].

Three mutually exclusive samples of events with tagged b jets are defined:

- 2b sample: Events in this sample must contain exactly two tight b jets and no medium b jets;
- 3b sample: Events in this sample must contain two jets that are tight b jets, a third jet that is either a tight or a medium b jet, and no other tight, medium, or loose b jet;
- 4b sample: Events in this sample must contain two jets that are tight b jets, a third jet that is either a tight or medium b jet, and a fourth jet that is either a tight, medium, or loose b jet.

The sample most sensitive to signal events is the 4b sample. The 3b sample is included to improve signal efficiency. The 2b sample is depleted in signal events and is used to help evaluate the background as described in Section 8.

5 Event simulation

Monte Carlo (MC) simulations of signal and background events are used to optimize selection criteria, validate analysis assumptions and performance, determine signal efficiency, evaluate systematic uncertainties, and conduct closure tests. In a closure test, the background evaluation procedures (Section 8) are applied to MC samples in order to demonstrate the ability of the procedures to correctly determine the known (MC) number of background events. Note that the background evaluation procedures themselves do not rely on simulation.

The principal classes of SM background events are described in the Introduction. Of these processes, all are simulated with the MADGRAPH 5.1.3.30 [29] event generator except for single-top-quark, WH, and ZH events, which are described using the POWHEG 301 [30] generator, and VV (diboson) and $\mathrm{t\bar{t}H}$ events, which are described using the PYTHIA 6.4.22 [31] generator. The SM processes are normalized to cross section calculations valid to the next-to-leading (NLO) or next-to-next-to-leading order [32–38], depending on availability, and otherwise to leading order.

For signal events, we assume that the $\widetilde{\chi}_1^0$, $\widetilde{\chi}_2^0$, and $\widetilde{\chi}_1^\pm$ states are pure higgsinos, and that any soft SM particles arising from the decays of the $\widetilde{\chi}_2^0$ and $\widetilde{\chi}_1^\pm$ states to the $\widetilde{\chi}_1^0$ state are too soft to be detected. For the purposes of event generation, we therefore take the $\widetilde{\chi}_1^0$ and $\widetilde{\chi}_2^0$ higgsinos to be mass-degenerate, consider $\widetilde{\chi}_1^0\widetilde{\chi}_2^0$ production only, and account for $\widetilde{\chi}_1^0\widetilde{\chi}_1^\pm$, $\widetilde{\chi}_2^0\widetilde{\chi}_1^\pm$, and $\widetilde{\chi}_1^\pm\widetilde{\chi}_1^\pm$ production through normalization of the cross section. Signal MC samples are generated for a range of higgsino mass values $m_{\widetilde{\chi}_1^0}$ using the MADGRAPH 5.1.5.4 generator, taking the LSP (gravitino) mass to be 1 GeV (i.e., effectively zero). The Higgs boson mass is set to 126 GeV. Up to two partons from initial-state radiation can be present, in addition to the higgsino pair. The decays of the $\widetilde{\chi}_1^0$ higgsinos are described using a pure phase-space matrix element. The signal event rates are normalized to the NLO cross section calculated with the PROSPINO2 pro-

gram [39].

For both signal and SM simulated events, the GEANT4 [40] package is used to model the detector and detector response. All MC samples incorporate the CTEQ6L1 or CTEQ6M [41, 42] parton distribution functions, with PYTHIA used to describe parton showering and hadronization. The MC distributions are corrected to account for pileup interactions, as observed in data. In addition, we correct the simulation so that the b-tagging and misidentification efficiencies match those determined from control samples in the data. The b-tagging efficiency correction factor depends slightly on jet p_{T} and has a typical value of 0.95 [27]. Corrections are applied to the signal samples so that the jet energy resolution matches that in data. A further correction, implemented as described in Appendix B of Ref. [43], accounts for mismodeling of initial-state radiation (ISR) in signal events.

6 Double-Higgs-boson selection

To reconstruct the two Higgs boson candidates in an event, we choose the four most b-quark-like jets based on the value of the CSV discriminating variable. These four jets can be grouped into three different pairs of Higgs boson candidates. Of the three possibilities, we choose the one with the smallest difference $|\Delta m_{jj}| \equiv |m_{jj,1} - m_{jj,2}|$ between the two candidate masses. Methods that use the known mass itself to select the best candidate tend to create an artificial peak in the background.

After choosing the two Higgs boson candidates, we calculate the distance $\Delta R \equiv \sqrt{(\Delta\phi)^2 + (\Delta\eta)^2}$ between the two jets for each $\mathrm{H} \to \mathrm{b\bar{b}}$ candidate decay. We call the larger of these two values ΔR_{max}. Higgs bosons in signal events generally exhibit a non-zero transverse boost, causing the two jets from the Higgs boson decay to have similar directions in the laboratory frame. As a consequence, both ΔR values and thus ΔR_{max} tend to be small. In contrast, for semileptonic $\mathrm{t\bar{t}}$ events, which represent the dominant background class in this analysis as mentioned above, three of the jets arise from a top quark that decays to three quarks via a hadronically decaying W boson while the fourth jet arises from a b quark from the semileptonic top-quark decay. Therefore three of the jets generally lie within the same hemisphere while the fourth jet lies in the opposite hemisphere. Thus one of the Higgs boson candidates is formed through the combination of jets from different hemispheres, making ΔR_{max} relatively large.

Double-Higgs-boson event candidates are selected using the variables $|\Delta m_{jj}|$, ΔR_{max}, and the average of the two Higgs boson candidate mass values $\langle m_{jj} \rangle \equiv (m_{jj,1} + m_{jj,2})/2$. Specifically, we require $|\Delta m_{jj}| < 20\,\mathrm{GeV}$, $\Delta R_{\mathrm{max}} < 2.2$, and $100 < \langle m_{jj} \rangle < 140\,\mathrm{GeV}$. The performance of the double-Higgs-boson reconstruction procedure for signal events is illustrated in Fig. 2.

The distributions of $|\Delta m_{jj}|$, ΔR_{max}, $\langle m_{jj} \rangle$, and $\mathcal{S}_{\mathrm{MET}}$ for events in the 4b event sample, after application of the above requirements (except for that on the displayed variable), are shown in Fig. 3.

7 Studies with background-enhanced data samples

This analysis marks the first time that the $\mathcal{S}_{\mathrm{MET}}$ variable has been used in a CMS SUSY study. To establish that the $\mathcal{S}_{\mathrm{MET}}$ variable does not exhibit unexpected features, we select two special samples, one enhanced in $\mathrm{t\bar{t}}$ background events and the other in QCD multijet background events, and compare the observed and predicted $\mathcal{S}_{\mathrm{MET}}$ distributions. Signal events contribute minimally to these two samples.

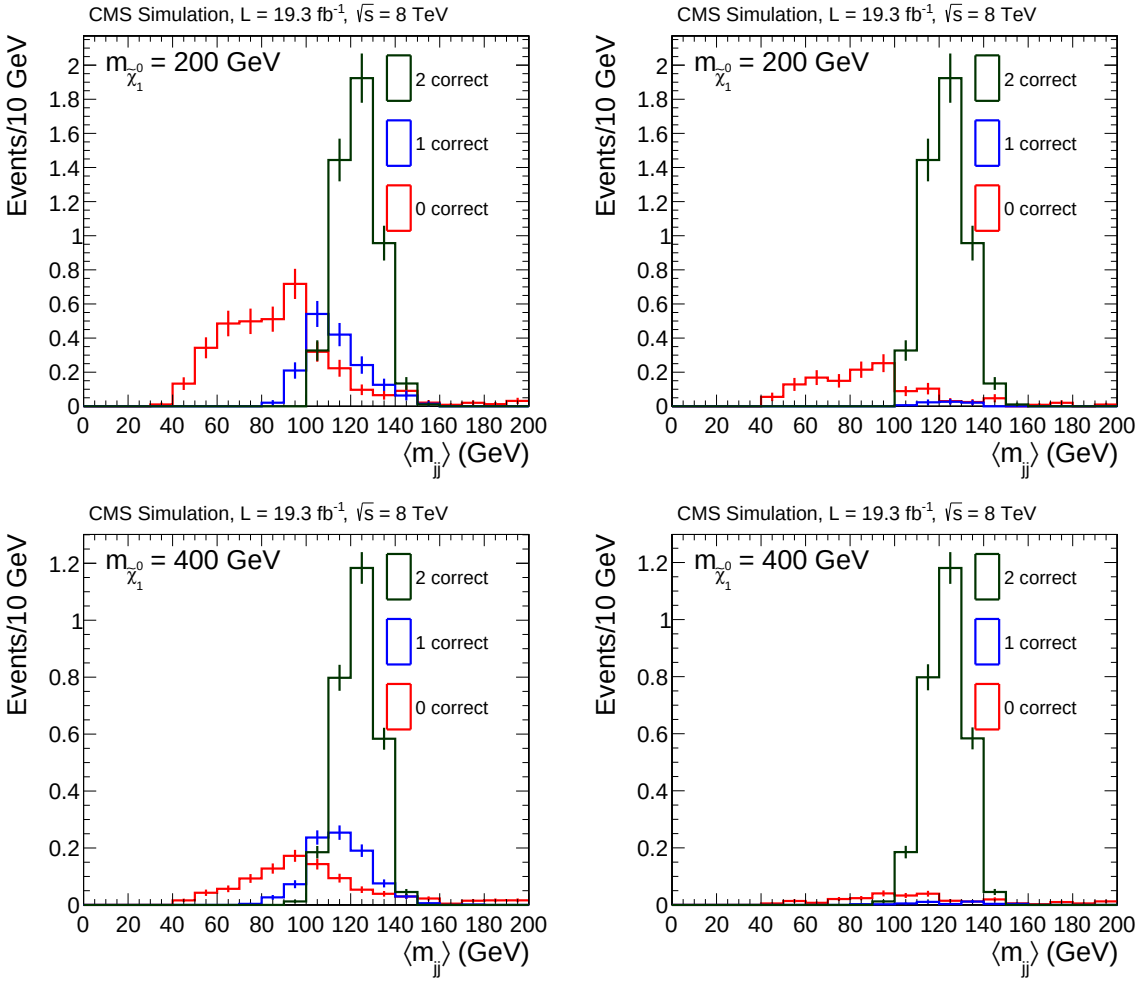

Figure 2: Distributions of reconstructed average mass $\langle m_{jj} \rangle$ for signal MC events in the 4b event sample for a (top row) 200 GeV and (bottom row) 400 GeV higgsino. Separate distributions are shown for the cases where zero, one, or two of the generator-level Higgs bosons are reconstructed correctly. The distributions are shown after all signal-region requirements are applied except for that on $\langle m_{jj} \rangle$. The left plots show the results for all signal MC events, while the right plots show the results for events in which each of the four generator-level quarks from the Higgs boson decays is matched with a reconstructed jet with $p_{\mathrm{T}} > 20$ GeV (in other words, for events where a correct double-Higgs-boson reconstruction is possible in this analysis).

The $\mathrm{t\bar{t}}$-background-enriched sample, referred to as the $\mathrm{t\bar{t}}$-BG sample, is selected by imposing the criteria of Section 3 except with an inversion of the electron or muon veto. Events in this sample are required to contain exactly one isolated electron or muon and at least two tight-tagged b jets. This sample allows us to study the $\mathcal{S}_{\mathrm{MET}}$ distribution of $\mathrm{t\bar{t}}$ events using selection criteria similar to those of the standard analysis. The QCD-background-enriched sample, referred to as the QCD-BG sample, is selected by imposing the criteria of Section 3 except without a requirement on $\Delta\phi_{\mathrm{min}}$. Events in this sample must contain at least two tight-tagged b jets.

Figure 4 presents the resulting distributions of $\mathcal{S}_{\mathrm{MET}}$. It is seen that the SM simulation describes the data reasonably well for both samples, with no evidence for an anomaly.

The $E_{\mathrm{T}}^{\mathrm{miss}}$ distribution of events in the QCD-BG sample is shown in Fig. 5. Comparing this distribution to the corresponding result for $\mathcal{S}_{\mathrm{MET}}$ [Fig. 4 (right)], it is seen that $\mathcal{S}_{\mathrm{MET}}$ is more

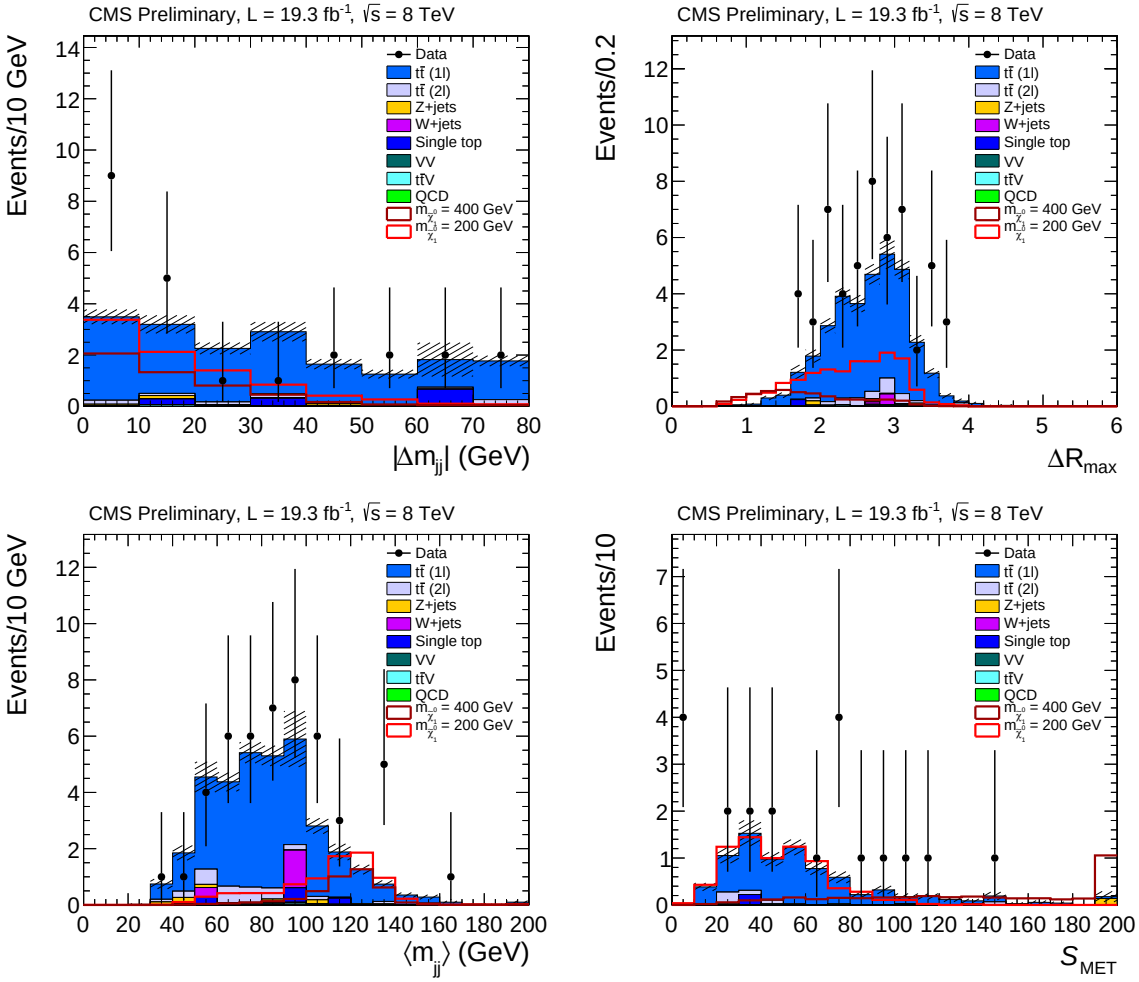

Figure 3: Distributions of events in the 4b sample, after all signal-region requirements are applied except for that on the displayed variable, in comparison with simulations of background and signal events: (top left) $|\Delta m_{jj}|$, (top right) ΔR_{max}, (bottom left) $\langle m_{jj} \rangle$, and (bottom right) $E_{\text{T}}^{\text{miss}}$-significance $\mathcal{S}_{\text{MET}}$. [$\text{t}\bar{\text{t}}$ (1l) and $\text{t}\bar{\text{t}}$ (2l) refer to $\text{t}\bar{\text{t}}$ events in which one or two top quarks decay semileptonically, respectively.] For the signal events, results are shown for higgsino masses of 200 and 400 GeV. The background distributions are stacked while the signal distributions are not. The hatched bands indicate the statistical uncertainty of the total SM simulated prediction.

effective at pulling QCD multijet events to smaller values of the respective variable, away from the signal region of high $E_{\text{T}}^{\text{miss}}$ or high $\mathcal{S}_{\text{MET}}$. This establishes that $\mathcal{S}_{\text{MET}}$ provides better separation between signal and background events than does $E_{\text{T}}^{\text{miss}}$, at least for background events in which large values of $E_{\text{T}}^{\text{miss}}$ (or $\mathcal{S}_{\text{MET}}$) arise because of detector mismeasurement.

8 Background evaluation

The SM background is evaluated using an algebraic method based entirely on data. The method relies on the tagged b-jet event samples introduced in Section 4.

A Higgs boson signal region (SIG) is defined by applying the selection criteria of Sections 3 and 6. For the $|\Delta m_{jj}|$ and $\langle m_{jj} \rangle$ variables, we therefore require:

- $|\Delta m_{jj}| < 20\,\text{GeV}$;

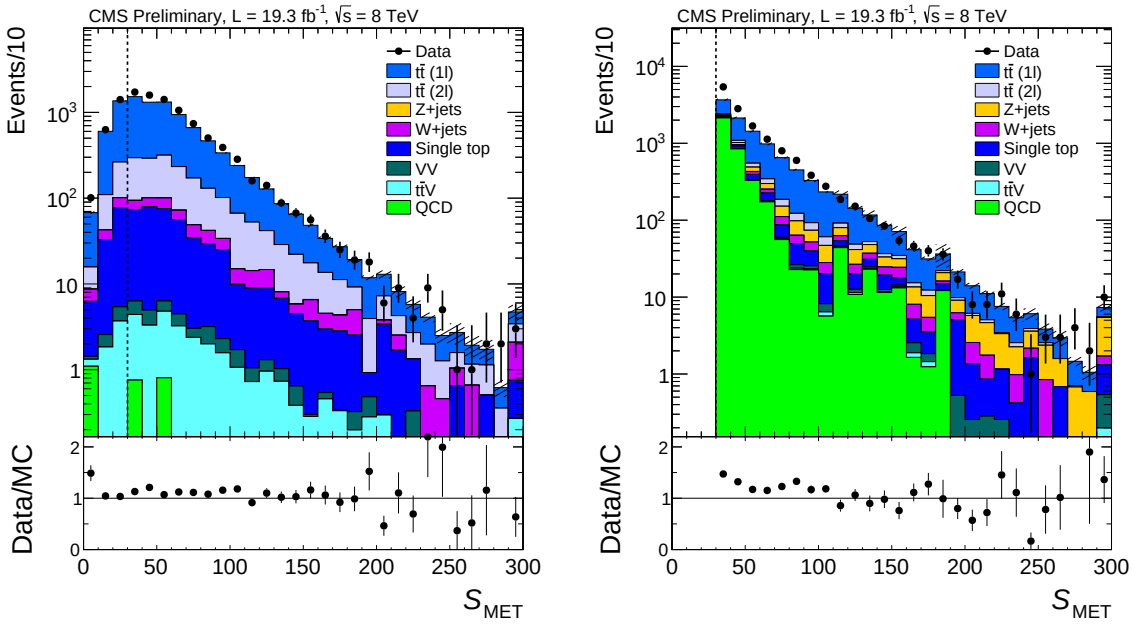

Figure 4: Distributions of $E_{\mathrm{T}}^{\mathrm{miss}}$-significance $\mathcal{S}_{\mathrm{MET}}$ in the (left) $\mathrm{t\bar{t}}$-BG and (right) QCD-BG background-enhanced event samples in comparison with simulations of background events. [$\mathrm{t\bar{t}}$ (1l) and $\mathrm{t\bar{t}}$ (2l) refer to $\mathrm{t\bar{t}}$ events in which one or two top quarks decay semileptonically, respectively.] The hatched bands indicate the statistical uncertainty of the total SM simulated prediction.

- $100 < \langle m_{jj} \rangle < 140\,\mathrm{GeV}$.

A sideband region (SB) is defined with these same criteria except using the region outside the following rectangle in the $|\Delta m_{jj}|$-$\langle m_{jj} \rangle$ plane:

- $|\Delta m_{jj}| < 30\,\mathrm{GeV}$;
- $90 < \langle m_{jj} \rangle < 150\,\mathrm{GeV}$.

The SIG and SB regions are illustrated in Fig. 6. One-dimensional projections are presented in Fig. 7.

Considering for purposes of illustration only the 4b and 2b samples, we define four observables, denoted A, B, C, and D:

- A: number of background events in the 4b-SIG region;
- B: number of background events in the 4b-SB region;
- C: number of background events in the 2b-SIG region;
- D: number of background events in the 2b-SB region.

We assume that the ratio of the number of events in the SIG region to that in the SB region, denoted the SIG/SB ratio, is the same for background events in the 2b and 4b samples. This assumption is supported by (for example) the similarity between the 2b and 4b results in the two top plots of Fig. 7. We further assume that the 2b-SIG and all SB regions are dominated by background, as is expected by design and as we validate with simulation. The prediction for the number of background events in the 4b-SIG region is then given by the algebraic expression $\mathrm{A} = (\mathrm{C}/\mathrm{D})\,\mathrm{B}$.

Considering next the 3b sample, also for purposes of illustration only, observables A and B are

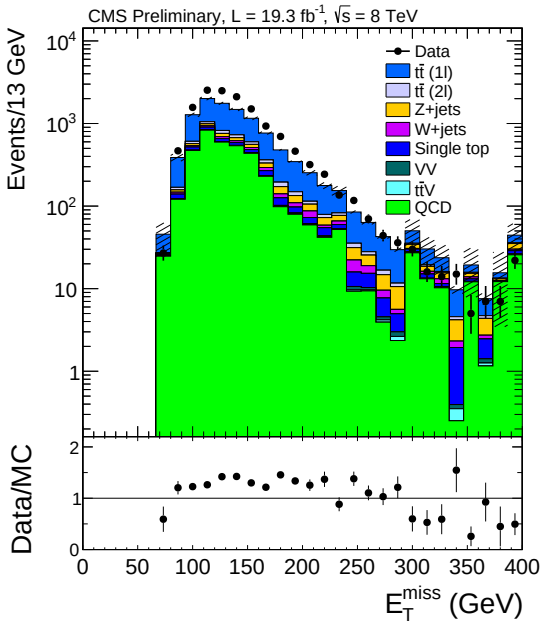

Figure 5: Distribution of $E_{\mathrm{T}}^{\mathrm{miss}}$ in the QCD-BG background-enhanced event sample in comparison with simulations of background events. [$\mathrm{t\bar{t}}$ (1l) and $\mathrm{t\bar{t}}$ (2l) refer to $\mathrm{t\bar{t}}$ events in which one or two top quarks decay semileptonically, respectively.] The hatched band indicates the statistical uncertainty of the total SM simulated prediction.

Table 1: Intervals of $E_{\mathrm{T}}^{\mathrm{miss}}$-significance $\mathcal{S}_{\mathrm{MET}}$ used in the analysis.

$\mathcal{S}_{\mathrm{MET}}$ bin 1	$30 < \mathcal{S}_{\mathrm{MET}} < 50$
$\mathcal{S}_{\mathrm{MET}}$ bin 2	$50 < \mathcal{S}_{\mathrm{MET}} < 100$
$\mathcal{S}_{\mathrm{MET}}$ bin 3	$100 < \mathcal{S}_{\mathrm{MET}} < 150$
$\mathcal{S}_{\mathrm{MET}}$ bin 4	$\mathcal{S}_{\mathrm{MET}} > 150$

taken to represent the number of events in the 3b-SIG and 3b-SB regions, respectively, while C and D are defined as before, viz., as the respective number of events in the 2b-SIG and 2b-SB regions. The prediction for the number of background events in the SIG region of the 3b sample is then given by the same expression as above, namely $\mathrm{A} = (\mathrm{C}/\mathrm{D})\,\mathrm{B}$.

In practice, the following procedure is used to evaluate the SM background. We examine the data in four intervals of $\mathcal{S}_{\mathrm{MET}}$, which are indicated in Table 1. The numbers of background events in the four $\mathcal{S}_{\mathrm{MET}}$ bins of the 2b-SIG, 3b-SIG, and 4b-SIG regions are determined simultaneously in a likelihood fit, with the SIG/SB ratios for background in all three b-jet samples constrained to a common value (determined in the fit) for each $\mathcal{S}_{\mathrm{MET}}$ bin separately. Figure 8 shows the predictions of the SM MC for the SIG/SB ratios, in the four bins of $\mathcal{S}_{\mathrm{MET}}$, for the three b-jet samples (for purposes of comparison, the data are also shown). It is seen that the SIG/SB ratio of SM events for $\mathcal{S}_{\mathrm{MET}}$ bin 1 is predicted to be about the same for all three b-jet samples, and similarly for the other three $\mathcal{S}_{\mathrm{MET}}$ bins, supporting the key assumption of the method. The systematic uncertainty associated with the background prediction accounts for potential differences between the SIG/SB ratios of background events in the different b-jet samples.

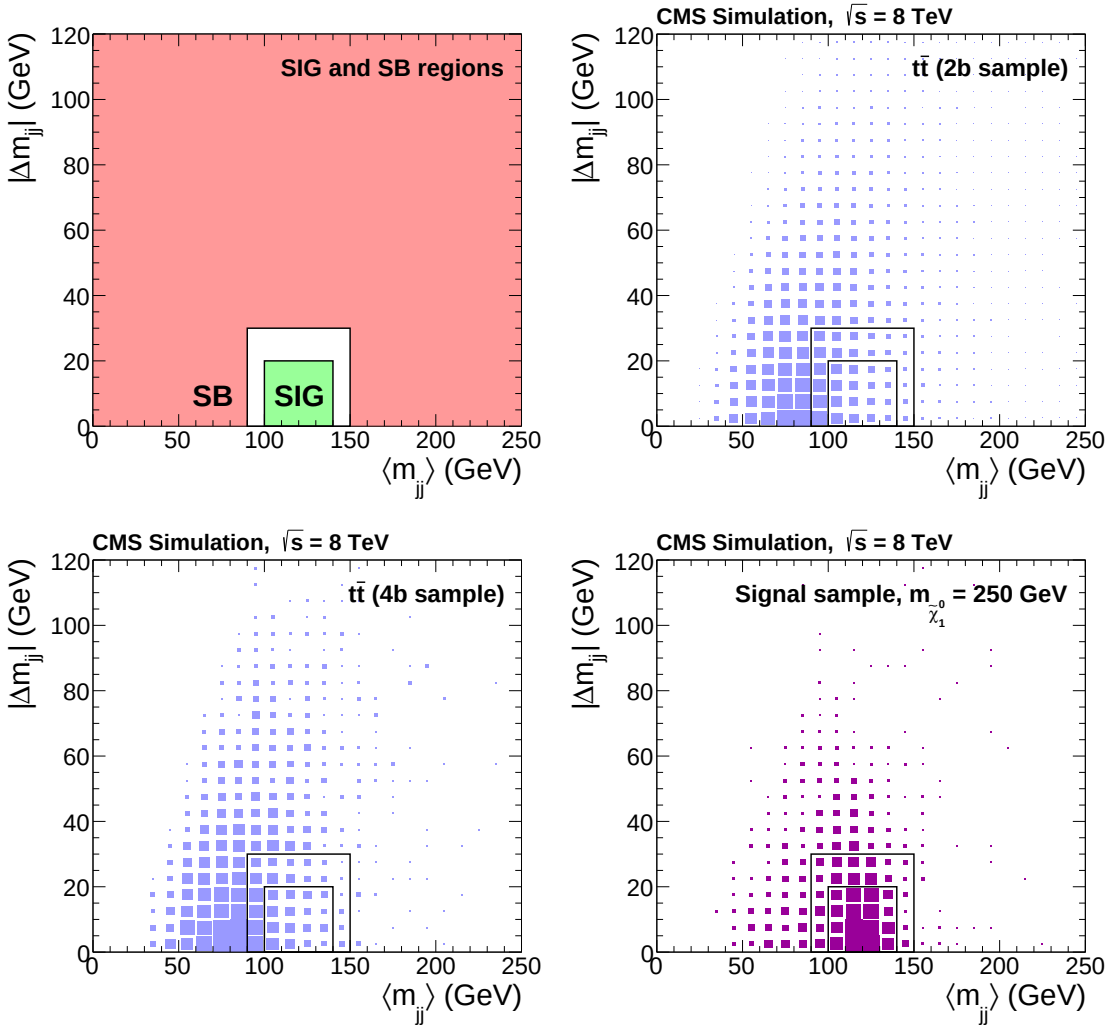

Figure 6: (top left) Illustration of the signal (SIG) and sideband (SB) regions in the $|\Delta m_{jj}|$ versus $\langle m_{jj} \rangle$ plane; (top right and bottom left) Distributions of simulated $\mathrm{t\bar{t}}$ events in the 2b and 4b samples; (bottom right) Distribution of simulated signal events in the 4b sample for a higgsino mass of 250 GeV. The plots employ an arbitrary integrated luminosity.

9 Systematic uncertainties

To evaluate the systematic uncertainty associated with the background estimate, we consider two terms, determined from simulation, which are treated as separate nuisance parameters in the likelihood fit. The first term, determined for each bin of $\mathcal{S}_{\mathrm{MET}}$ in the 4b (3b) sample, is given by the larger of the following: the difference from unity of the double ratio R, with R the SIG/SB ratio of 4b (3b) events divided by the SIG/SB ratio of 2b events ("non-closure result"), or the statistical uncertainty of R. The size of this uncertainty varies between around 14 and 40%, with a typical value of 25%. The second term accounts for potential differences between the SIG/SB ratio of $\mathrm{t\bar{t}}$ and QCD multijet events as well as for the possibility that the relative fraction of $\mathrm{t\bar{t}}$ and QCD multijet events varies between the 2b, 3b, and 4b samples or bins of $\mathcal{S}_{\mathrm{MET}}$. From simulation, the relative fraction of background events due to QCD multijet events varies by 6% (between 1 and 7%), depending primarily on the bin of $\mathcal{S}_{\mathrm{MET}}$. We conservatively allow up to a 20% variation in this fraction and determine a corresponding 7% increase in the non-closure result, which we define as the associated uncertainty.

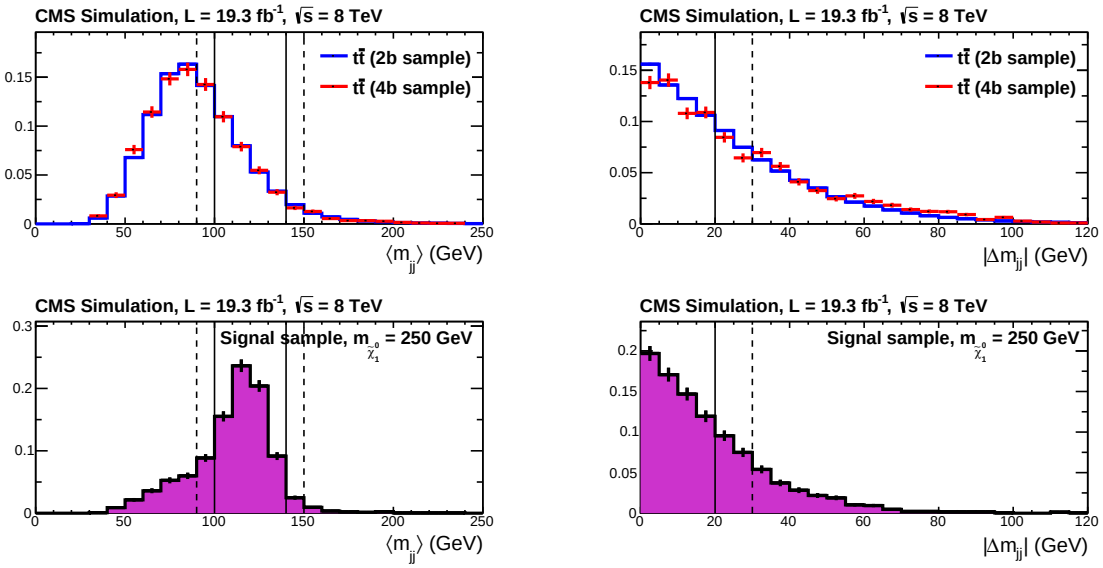

Figure 7: One-dimensional projections of (left) $\langle m_{jj} \rangle$ and (right) $|\Delta m_{jj}|$ for simulated (top) $\mathrm{t\bar{t}}$ and (bottom) signal events, with a higgsino mass of 250 GeV. For $\mathrm{t\bar{t}}$ events (signal events), results are shown for the 2b and 4b samples (4b sample). The solid and dashed vertical lines indicate the boundaries of the signal (SIG) and sideband (SB) regions, respectively. The distributions are normalized to unit area.

Table 2: Typical values of the systematic uncertainty for signal efficiency, in percentage, for a higgsino mass of 200 or 400 GeV.

Source	200 GeV	400 GeV
Jet energy scale	5-10%	5%
Jet energy resolution	2-4%	2%
Pileup modeling	4%	1%
Trigger efficiency	1-2%	1-2%
b-tagging efficiency	10%	10%
ISR modeling	1%	1%
Parton distribution functions	1%	1%
Luminosity	2.6%	2.6%

As a cross check, we vary the rate of gluon splitting to a $\mathrm{b\bar{b}}$ pair in the simulation and adjust the top-quark p_{T} spectrum to match data. We observe negligible effects on the evaluated uncertainty.

Systematic uncertainties associated with the signal efficiency arise from various sources. An uncertainty associated with the jet energy scale is evaluated by varying this scale by its p_{T}- and η-dependent uncertainties. The uncertainties associated with the jet energy resolution, pileup modeling, trigger efficiency, b-tagging efficiency correction factor, and ISR modeling, are evaluated by varying the respective quantities by their uncertainties. Systematic uncertainties associated with the parton distribution functions are evaluated [41, 44, 45] following the recommendations of Ref. [46]. The uncertainty of the luminosity determination is 2.6% [47]. The uncertainties are evaluated individually for the different $\mathcal{S}_{\mathrm{MET}}$ bins, for both the SB and SIG regions, and for each of the 2b, 3b, and 4b samples, with correlations taken into account. Table 2 lists typical values of the uncertainties.

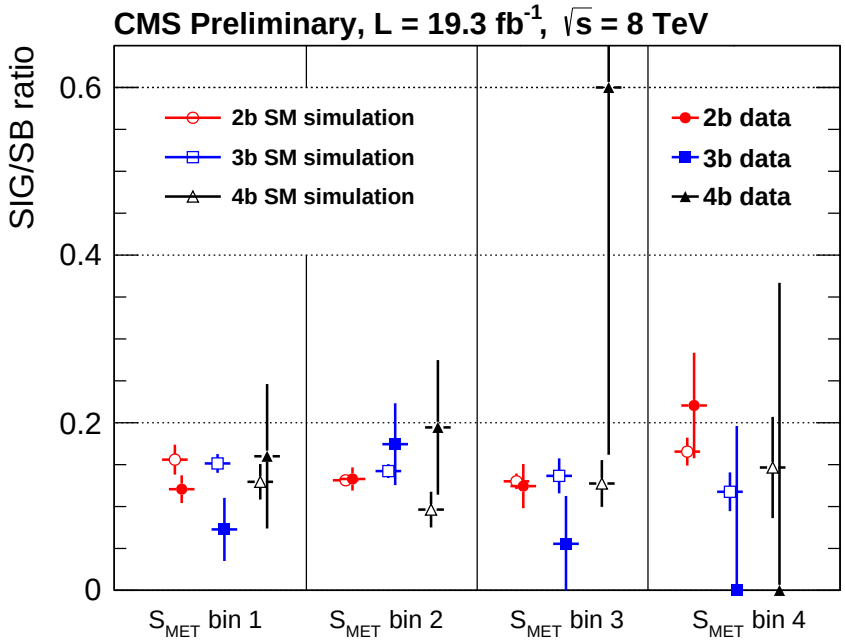

Figure 8: The ratio of the number of events in the signal (SIG) region to that in the sideband (SB) region as a function of $\mathcal{S}_{\mathrm{MET}}$ bin (see Table 1), for the 2b, 3b, and 4b event samples. The results for the simulation account for the various SM processes.

10 Likelihood analysis

A likelihood function is constructed using the RooFit [48] package. There are three b-jet samples in the analysis (Section 4), each with a SIG and SB region that is divided into four intervals of $\mathcal{S}_{\mathrm{MET}}$ (Table 1). This yields 24 mutually exclusive observables. Each observable is described by a Poissonian distribution in the likelihood function. A lognormal constraint probability distribution function (PDF) accounts for each systematic uncertainty term (nuisance parameter) except for the b-tagging-efficiency-correction term, which is constrained by a Gaussian PDF.

The Poisson mean for observable j is the sum of the background (BG) and signal (SUSY) contributions, which we express as:

$$n_j \;=\; \mu_j^{BG} + r \cdot s_j^{SUSY} \cdot \mu_{0;j}^{SUSY}, \tag{1}$$

where $\mu_{0;j}^{SUSY}$ is the expected SUSY contribution for the predicted cross section, s_j^{SUSY} is the total systematic uncertainty for signal events, and r is a signal strength parameter. The background estimate is expressed in the likelihood function through the following relations:

$$\mu_{4bSIG,i}^{BG} \;=\; s_{4b,i}^{BG} \cdot R_i \cdot \mu_{4bSB,i}^{BG}, \tag{2}$$

$$\mu_{3bSIG,i}^{BG} \;=\; s_{3b,i}^{BG} \cdot R_i \cdot \mu_{3bSB,i}^{BG}, \tag{3}$$

$$\mu_{2bSIG,i}^{BG} \;=\; R_i \cdot \mu_{2bSB,i}^{BG}, \tag{4}$$

where i denotes the $\mathcal{S}_{\mathrm{MET}}$ bin (1 to 4), R_i is the common SIG/SB ratio for that bin, and $s_{4b,i}$ and $s_{3b,i}$ represent the systematic uncertainties of the background estimate for the 4b and 3b samples, respectively. The parameters with values determined by the fit are listed in Table 3.

To evaluate the discovery sensitivity of the analysis, we construct test data sets for different higgsino masses, with the values of the observables fixed to the sum of the MC predictions for background and signal. Figure 9 shows the corresponding null-hypothesis p values, along

Table 3: Parameters with values determined by the likelihood fit.

Parameter	Number of parameters	Constraint PDF
$\mu^{BG}_{kbSB,i}$	(3 b tag samples) $\times$ (4 $\mathcal{S}_{\mathrm{MET}}$ bins) = 12	None
$s^{BG}_{kb,i}$	(2 b tag samples) $\times$ (4 $\mathcal{S}_{\mathrm{MET}}$ bins) = 8	Lognormal
s^{SUSY}_{j}	(3 b tag samples) $\times$ (4 $\mathcal{S}_{\mathrm{MET}}$ bins) $\times$ (SIG and SB) = 24	Lognormal
R_i	4 $\mathcal{S}_{\mathrm{MET}}$ bins	None
r	1 signal normalization	None

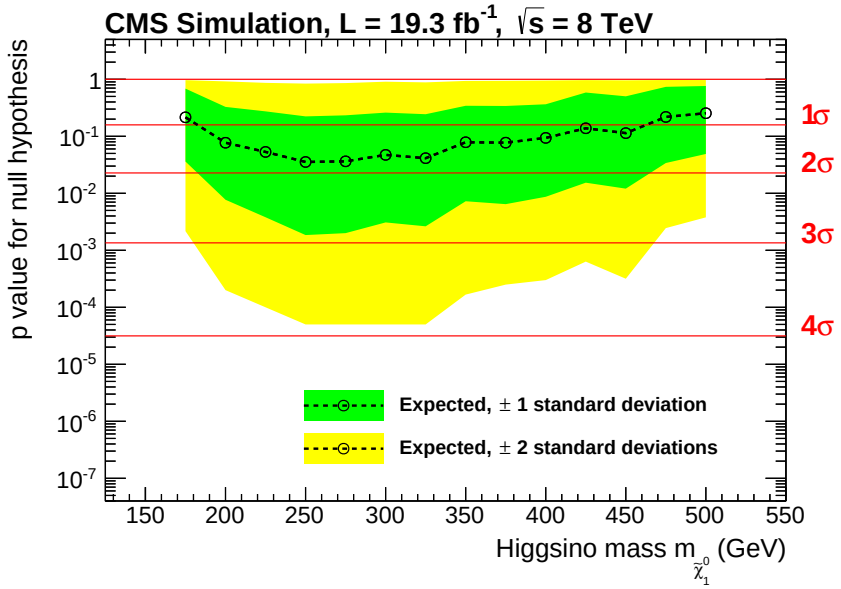

Figure 9: Expected p values for the null hypothesis (no SUSY) should a higgsino signal be present with the predicted cross section. The green and yellow bands indicate the one- and two-standard deviation intervals, and the horizontal solid (red) lines the sensitivity to a SUSY signal in standard deviations.

with the corresponding expected signal significance expressed in standard deviations. The results are based on a frequentist calculator and a one-sided profile-likelihood test statistic. The expected sensitivity approaches two standard deviations for higgsino masses of about 260 GeV.

11 Results

The observed numbers of events in the 3b-SIG and 4b-SIG regions are shown in Fig. 10 in comparison with the SM background predictions from the likelihood fit. Numerical values are given in Table 4. The data are seen to be consistent with the SM predictions to within the uncertainties. Thus, we do not observe evidence for higgsinos. For purposes of illustration, the expected signal distributions for higgsino masses of 250 and 400 GeV are included in Fig. 10. Figure 11 shows the data in comparison with predictions from SM simulation.

Figure 12 (top) presents the expected and observed 95% confidence-level (CL) upper limits on the signal strength as a function of the higgsino mass. A signal strength $r = 1$ corresponds to the predicted cross section, and points below $r = 1$ are excluded. Assuming the absence

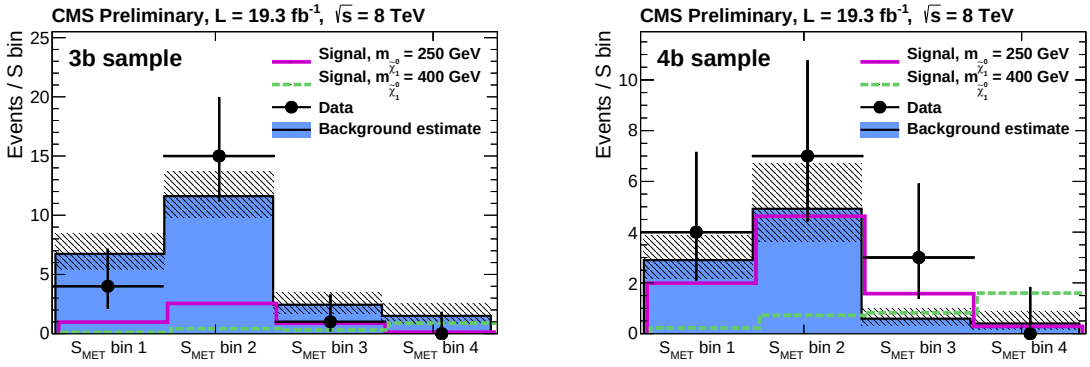

Figure 10: Observed numbers of events in the (left) 3b-SIG and (right) 4b-SIG regions, in bins of $E_{\mathrm{T}}^{\mathrm{miss}}$-significance $\mathcal{S}_{\mathrm{MET}}$, in comparison with the SM background estimates from the likelihood fit. The hatched bands show the total uncertainty of the background prediction, with statistical and systematic terms combined. The (unstacked) results for signal events, with a higgsino mass of either 250 or 400 GeV, are also shown.

Table 4: Observed numbers of events and corresponding SM background estimates from the likelihood fit for the 3b-SIG and 4b-SIG regions. For the data, the first uncertainty is statistical and the second systematic.

$\mathcal{S}_{\mathrm{MET}}$ bin	$\mathcal{S}_{\mathrm{MET}}$ range	SM background (3b-SIG)	Data (3b-SIG)	SM background (4b-SIG)	Data (4b-SIG)
1	$30 < \mathcal{S}_{\mathrm{MET}} < 50$	$6.7^{+1.4+1.0}_{-1.1-0.7}$	4	$2.9^{+0.8+0.5}_{-0.6-0.4}$	4
2	$50 < \mathcal{S}_{\mathrm{MET}} < 100$	$11.6^{+1.9+0.9}_{-1.6-0.7}$	15	$4.9^{+1.1+1.4}_{-0.9-0.9}$	7
3	$100 < \mathcal{S}_{\mathrm{MET}} < 150$	$2.44^{+0.84+0.56}_{-0.64-0.35}$	1	$0.59^{+0.39+0.09}_{-0.26-0.09}$	3
4	$\mathcal{S}_{\mathrm{MET}} > 150$	$1.50^{+0.82+0.64}_{-0.54-0.32}$	0	$0.40^{+0.39+0.26}_{-0.22-0.10}$	0

of SUSY, the expected cross section upper limits reach the level of the predicted cross section for higgsino masses between around 270 and 350 GeV. However, because of a slight excess of data events compared to the background expectation [see, e.g., Fig. 10 (right)], we are unable to exclude the signal hypothesis for any value of higgsino mass. Figure 12 (bottom) expresses the results in terms of the signal model cross section.

12 Summary

A search is presented for the electroweak pair production of higgsinos in proton-proton collisions at 8 TeV, based on the gauge-mediated-SUSY-breaking scenario of Ref. [18]. The data sample was collected with the CMS detector in 2012, corresponding to an integrated luminosity of 19.3 fb^{-1}. Each higgsino is presumed to decay to an almost-massless lightest-supersymmetric particle, which escapes without detection, and to a Higgs boson. The Higgs boson is considered in its most likely decay mode, namely to a bottom quark-antiquark pair. The analysis is based on the reconstruction of the two Higgs bosons and on the missing-transverse-energy-significance variable $\mathcal{S}_{\mathrm{MET}}$. The background from standard model processes, which principally arises from events with a top quark-antiquark pair in which one top quark decays hadronically while the other decays semileptonically, is evaluated using control samples in the data. The results are obtained using a global likelihood fit in which the numbers of events in 24 exclusive

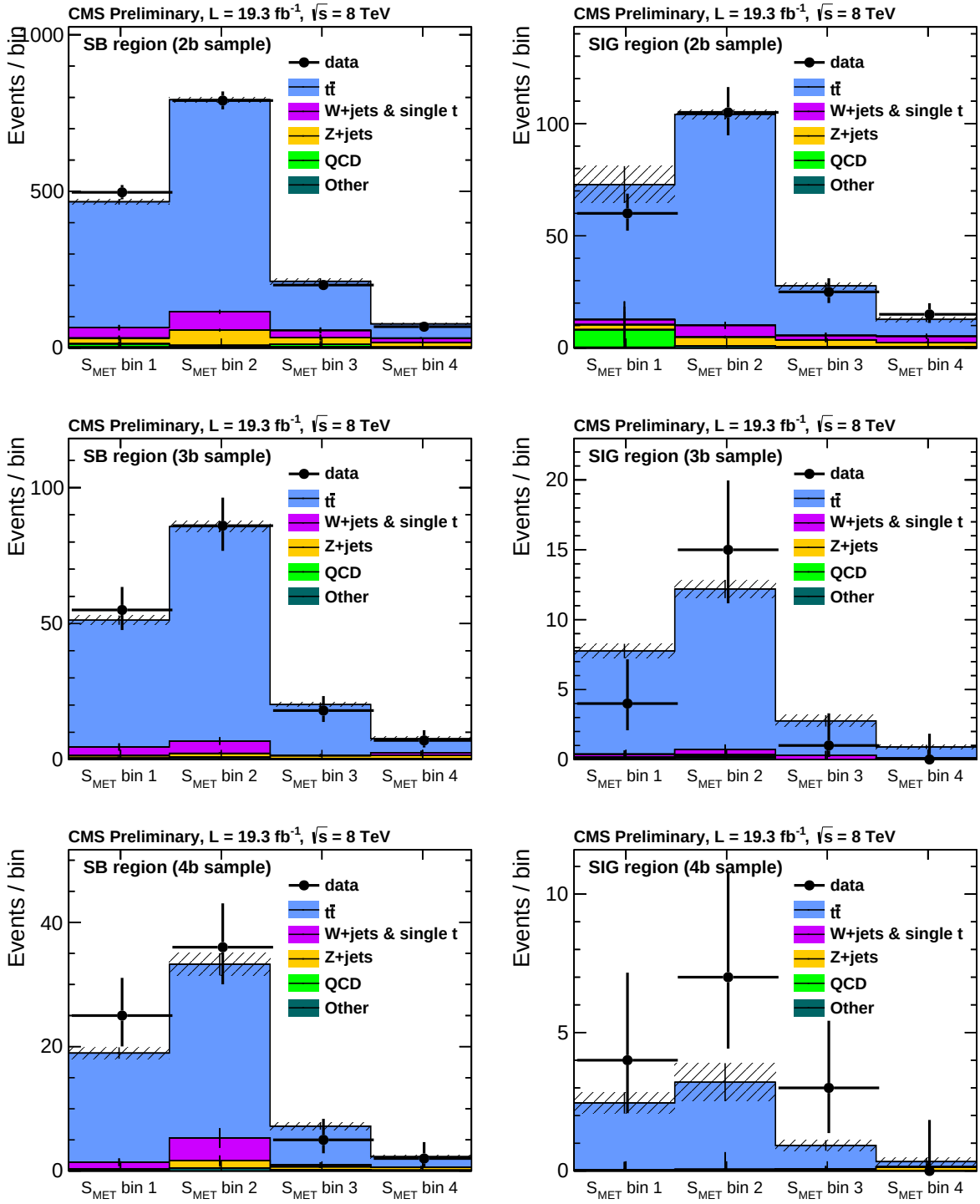

Figure 11: Observed numbers of events in bins of $E_{\mathrm{T}}^{\mathrm{miss}}$-significance $\mathcal{S}_{\mathrm{MET}}$ and corresponding prediction from SM simulation for the sideband SB (left) and signal SIG (right) regions, for the 2b (top), 3b (middle), and 4b (bottom) event samples. The hatched bands indicate the statistical uncertainty of the total SM simulated prediction.

bins in a three-dimensional array of $\mathcal{S}_{\mathrm{MET}}$, signal and sideband intervals in the Higgs-boson-mass variables, and tagged bottom-quark jet samples, are simultaneously examined. For higgsino masses between around 270 and 350 GeV, the expected cross section upper limits reach the level of the expected production cross section. Because of a slight excess in the observed number of events compared to the estimated background, we are unable to exclude the signal model for any value of higgsino mass.

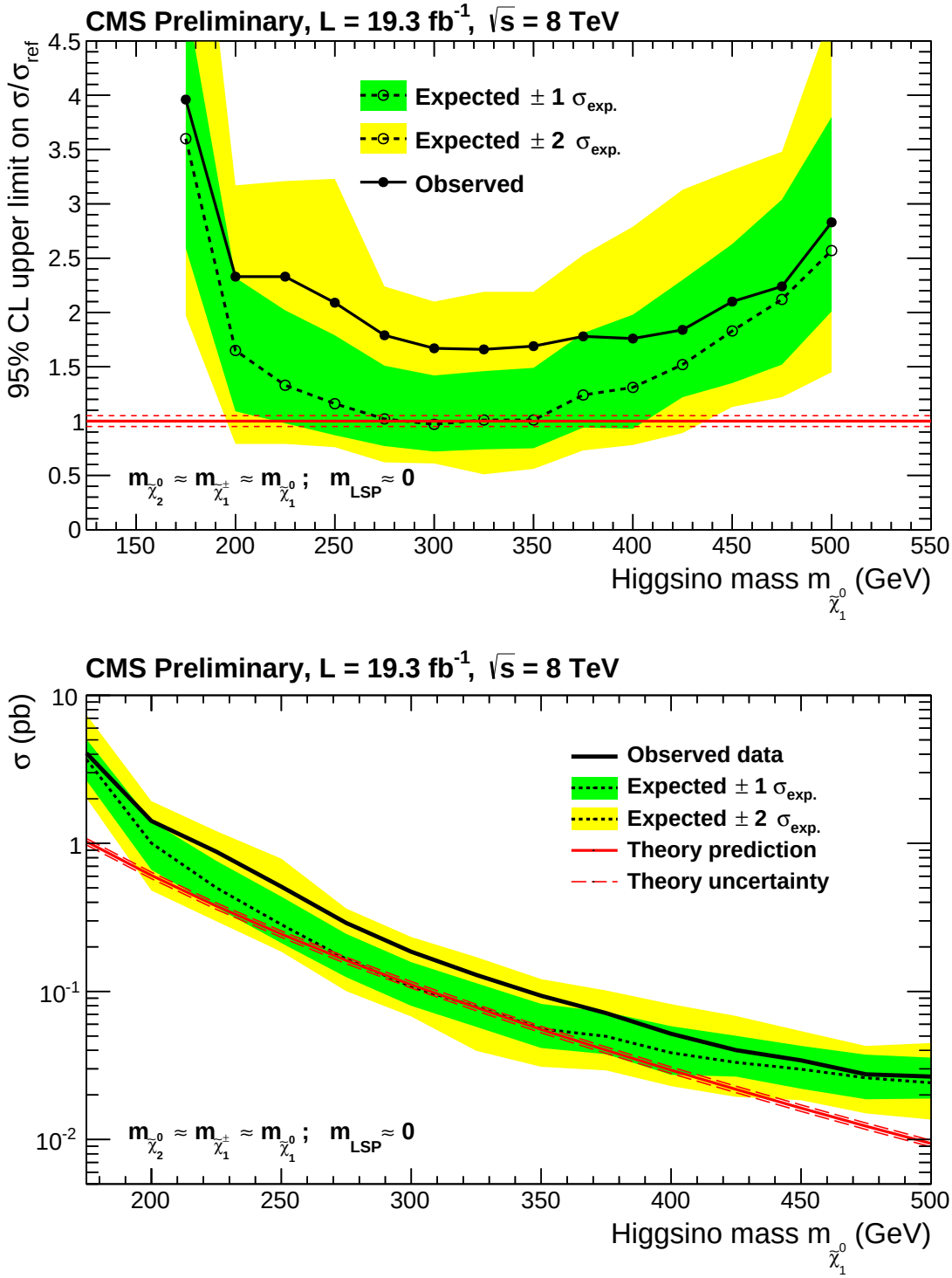

Figure 12: Observed and expected upper limits on the (top) signal strength normalized to the reference cross section, and (bottom) cross section, as a function of higgsino mass. The uncertainty associated with the theory cross section is 5%. The green and yellow bands indicate the one- and two-standard deviation intervals, respectively, for the expected result.

References

[1] P. Ramond, "Dual theory for free fermions", *Phys. Rev. D* **3** (1971) 2415, doi:10.1103/PhysRevD.3.2415.

[2] Y. A. Golfand and E. P. Likhtman, "Extension of the algebra of Poincaré group generators and violation of P invariance", *JETP Lett.* **13** (1971) 323.

[3] A. Neveu and J. H. Schwarz, "Factorizable dual model of pions", *Nucl. Phys. B* **31** (1971) 86, doi:10.1016/0550-3213(71)90448-2.

[4] D. V. Volkov and V. P. Akulov, "Possible universal neutrino interaction", *JETP Lett.* **16** (1972) 438.

[5] J. Wess and B. Zumino, "A Lagrangian model invariant under supergauge transformations", *Phys. Lett. B* **49** (1974) 52, doi:10.1016/0370-2693(74)90578-4.

[6] J. Wess and B. Zumino, "Supergauge transformations in four dimensions", *Nucl. Phys. B* **70** (1974) 39, doi:10.1016/0550-3213(74)90355-1.

[7] P. Fayet, "Supergauge invariant extension of the Higgs mechanism and a model for the electron and its neutrino", *Nucl. Phys. B* **90** (1975) 104, doi:10.1016/0550-3213(75)90636-7.

[8] H. P. Nilles, "Supersymmetry, supergravity and particle physics", *Phys. Rep.* **110** (1984) 1, doi:10.1016/0370-1573(84)90008-5.

[9] S. Dimopoulos and G. F. Giudice, "Naturalness constraints in supersymmetric theories with nonuniversal soft terms", *Phys. Lett. B* **357** (1995) 573, doi:10.1016/0370-2693(95)00961-J, arXiv:hep-ph/9507282.

[10] R. Barbieri and D. Pappadopulo, "S-particles at their naturalness limits", *JHEP* **10** (2009) 061, doi:10.1088/1126-6708/2009/10/061, arXiv:0906.4546.

[11] M. Papucci, J. T. Ruderman, and A. Weiler, "Natural SUSY endures", *JHEP* **09** (2012) 035, doi:10.1007/JHEP09(2012)035, arXiv:1110.6926.

[12] CMS Collaboration, "Observation of a new boson with mass near 125 GeV in pp collisions at $\sqrt{s}$ = 7 and 8 TeV", *JHEP* **06** (2013) 081, doi:10.1007/JHEP06(2013)081, arXiv:1303.4571.

[13] ATLAS Collaboration, "Observation of a new particle in the search for the standard model Higgs boson with the ATLAS detector at the LHC", *Phys. Lett. B* **716** (2012) 1, doi:10.1016/j.physletb.2012.08.020, arXiv:1207.7214.

[14] CMS Collaboration, "Observation of a new boson at a mass of 125 GeV with the CMS experiment at the LHC", *Phys. Lett. B* **716** (2012) 30, doi:10.1016/j.physletb.2012.08.021, arXiv:1207.7235.

[15] CMS Collaboration, "Search for stop and higgsino production using diphoton Higgs boson decays", (2013). arXiv:1312.3310. Submitted to *Phys. Rev. Lett.*

[16] CMS Collaboration, "Search for electroweak production of charginos and neutralinos in final states with a Higgs boson in pp collisions at $\sqrt{s} = 8$ TeV", CMS Physics Analysis Summary CMS-PAS-SUS-13-017, 2013.

[17] ATLAS Collaboration, "Search for chargino and neutralino production in final states with one lepton, two b-jets consistent with a Higgs boson, and missing transverse momentum with the ATLAS detector in 20.3 fb^{-1} of $\sqrt{s} = 8$ TeV pp collisions", ATLAS Note ATLAS-CONF-2013-093, 2013.

[18] K. T. Matchev and S. D. Thomas, "Higgs and Z boson signatures of supersymmetry", *Phys. Rev. D* **62** (2000) 077702, doi:10.1103/PhysRevD.62.077702, arXiv:hep-ph/9908482.

[19] J. T. Ruderman and D. Shih, "General neutralino NLSPs at the early LHC", *JHEP* **08** (2012) 159, doi:10.1007/JHEP08(2012)159, arXiv:1103.6083.

[20] S. Dittmaier et al., "Handbook of LHC Higgs cross sections: 1. inclusive observables", (2011). arXiv:1101.0593.

[21] CMS Collaboration, "Missing transverse energy performance of the CMS detector", *JINST* **6** (2011) P09001, doi:10.1088/1748-0221/6/09/P09001, arXiv:1106.5048.

[22] CMS Collaboration, "The CMS experiment at the CERN LHC", *JINST* **3** (2008) S08004, doi:10.1088/1748-0221/3/08/S08004.

[23] CMS Collaboration, "Particle flow event reconstruction in CMS and performance for jets, taus and $E_{\mathrm{T}}^{\mathrm{miss}}$", CMS Physics Analysis Summary CMS-PAS-PFT-09-001, 2009.

[24] CMS Collaboration, "Performance of tau-lepton reconstruction and identification in CMS", *JINST* **7** (2012) P01001, doi:10.1088/1748-0221/7/01/P01001, arXiv:1109.6034.

[25] M. Cacciari, G. P. Salam, and G. Soyez, "The anti-k_t jet clustering algorithm", *JHEP* **04** (2008) 063, doi:10.1088/1126-6708/2008/04/063, arXiv:0802.1189.

[26] M. Cacciari and G. P. Salam, "Pileup subtraction using jet areas", *Phys. Lett. B* **659** (2008) 119, doi:10.1016/j.physletb.2007.09.077, arXiv:0707.1378.

[27] CMS Collaboration, "Identification of b-quark jets with the CMS experiment", *JINST* **8** (2013) P04013, doi:10.1088/1748-0221/8/04/P04013, arXiv:1211.4462.

[28] CMS Collaboration, "Performance of b tagging at $\sqrt{s} = 8$ TeV in multijet, $\mathrm{t\bar{t}}$ and boosted topology events,", CMS Physics Analysis Summary CMS-PAS-BTV-13-001, 2013.

[29] J. Alwall et al., "MadGraph5: going beyond", *JHEP* **06** (2011) 128, doi:10.1007/JHEP06(2011)128, arXiv:1106.0522.

[30] S. Frixione, P. Nason, and C. Oleari, "Matching NLO QCD computations with parton shower simulations: the POWHEG method", *JHEP* **11** (2007) 070, doi:10.1088/1126-6708/2007/11/070, arXiv:0709.2092.

[31] T. Sjöstrand, S. Mrenna, and P. Skands, "PYTHIA 6.4 physics and manual", *JHEP* **05** (2006) 026, doi:10.1088/1126-6708/2006/05/026, arXiv:hep-ph/0603175.

[32] S. Frixione and B. R. Webber, "Matching NLO QCD computations and parton shower simulations", *JHEP* **06** (2002) 029, doi:10.1088/1126-6708/2002/06/029, arXiv:hep-ph/0204244.

[33] S. Frixione, P. Nason, and B. R. Webber, "Matching NLO QCD and parton showers in heavy flavor production", *JHEP* **08** (2003) 007, doi:10.1088/1126-6708/2003/08/007, arXiv:hep-ph/0305252.

[34] N. Kidonakis, "Differential and total cross sections for top pair and single top production", (2012). arXiv:1205.3453.

[35] J. M. Campbell and R. K. Ellis, "$t\bar{t}W^{\pm}$ production and decay at NLO", *JHEP* **07** (2012) 052, doi:10.1007/JHEP07(2012)052, arXiv:1204.5678.

[36] M. Garzelli, A. Kardos, C. Papadopoulos, and Z. Trocsanyi, "$t\bar{t}W^{\pm}$ and $t\bar{t}Z$ hadroproduction at NLO accuracy in QCD with parton shower and hadronization effects", *JHEP* **11** (2012) 056, doi:10.1007/JHEP11(2012)056, arXiv:1208.2665.

[37] J. M. Campbell, R. K. Ellis, and C. Williams, "Vector boson pair production at the LHC", *JHEP* **07** (2011) 018, doi:10.1007/JHEP07(2011)018, arXiv:1105.0020.

[38] R. Gavin, Y. Li, F. Petriello, and S. Quackenbush, "W Physics at the LHC with FEWZ 2.1", *Comput. Phys. Commun.* **184** (2013) 208, doi:10.1016/j.cpc.2012.09.005, arXiv:1201.5896.

[39] W. Beenakker et al., "The production of charginos/neutralinos and sleptons at hadron colliders", *Phys. Rev. Lett.* **83** (1999) 3780, doi:10.1103/PhysRevLett.100.029901,10.1103/PhysRevLett.83.3780, arXiv:hep-ph/9906298.

[40] S. Agostinelli et al., "GEANT4 — a simulation toolkit", *Nucl. Instr. and Meth. A* **506** (2003) 250, doi:10.1016/S0168-9002(03)01368-8.

[41] J. Pumplin et al., "New generation of parton distributions with uncertainties from global QCD analysis", *JHEP* **07** (2002) 012, doi:10.1088/1126-6708/2002/07/012, arXiv:hep-ph/0201195.

[42] P. M. Nadolsky et al., "Implications of CTEQ global analysis for collider observables", *Phys. Rev. D* **78** (2008) 013004, doi:10.1103/PhysRevD.78.013004, arXiv:0802.0007.

[43] CMS Collaboration, "Search for top-squark pair production in the single-lepton final state in pp collisions at $\sqrt{s} = 8$ TeV", *Eur. Phys. J. C* **73** (2013) 2677, doi:10.1140/epjc/s10052-013-2677-2, arXiv:1308.1586.

[44] A. D. Martin, W. J. Stirling, R. S. Thorne, and G. Watt, "Parton distributions for the LHC", *Eur. Phys. J. C* **63** (2009) 189, doi:10.1140/epjc/s10052-009-1072-5, arXiv:0901.0002.

[45] R. D. Ball et al., "Impact of heavy quark masses on parton distributions and LHC phenomenology", *Nucl. Phys. B* **849** (2011) 296, doi:10.1016/j.nuclphysb.2011.03.021, arXiv:1101.1300.

[46] M. Botje et al., "The PDF4LHC working group interim recommendations", (2011). arXiv:1101.0538.

[47] CMS Collaboration, "CMS luminosity based on pixel cluster counting – summer 2013 update", CMS Physics Analysis Summary CMS-PAS-LUM-13-001, 2013.

[48] W. Verkerke and D. P. Kirkby, "The RooFit toolkit for data modeling", (2003). arXiv:physics/0306116.